

ON THE PERFORMANCE OF VERTICAL AXIS WIND TURBINES IN STEADY WIND UNDER VARIOUS BLADE CAMBER LEVELS

Michael De Los Santos Bausas¹ and Louis Angelo Danao^{1,2}

¹Energy Engineering Program, University of the Philippines, Diliman, Quezon City, Philippines, e-mail: michaelbausas@gmail.com

²Department of Mechanical Engineering, University of the Philippines, Diliman, Quezon City, Philippines, e-mail: louisdanao@gmail.com

Received Date: February, 26 2015

Nomenclature

α	angle of attack	P_B	blade power (three blades)
λ	tip speed ratio, $Rt/Uip\theta$ azimuth position	P_w	wind power
ρ	air density	R	rotor radius
ω	rotor angular speed	Re	blade Reynolds number
A	rotor frontal swept area, 2RL, (in hotwire anemometry, constant 1)	T_b	blade torque (single blade)
c	blade chord	T_B	blade torque (three blades)
C_d	drag coefficient	U_∞	free stream wind speed
$C_{d,ss}$	static stall drag coefficient	V	characteristic wind velocity
C_l	lift coefficient	V_b	blade velocity, $R\omega$
$C_{l,ss}$	static stall lift coefficient	W	relative velocity of wind with respect to blade
C_m	moment coefficient	XX	maximum blade thickness in percent chord
CP	power coefficient	y^+	dimensionless wall distance
ΔCP	change in CP	BEM	Blade Element/Momentum
D	rotor diameter	CFD	Computational Fluid Dynamics
F_d	drag force	HAWT	Horizontal Axis Wind Turbine
F_l	lift force	RANS	Reynolds Averaged Navier–Stokes

Abstract

Vertical axis wind turbine (VAWT) has been shown to be more suited to small scale power production in the urban environment due to distinct advantages over its horizontal counterpart. Over the last few years, continuous improvement on its aerodynamic performance, either through experimental or numerical analysis, have been carried out by numerous researchers. VAWT performance was investigated using Computational Fluid Dynamics modeling. The influence of camber on steady wind performance was analyzed and the most efficient of all levels of blade camber studied for VAWT application was determined. Various levels of camber were imposed on to a NACA XX25 blade profile, namely: 0.5%; 1.5% (cambered close to the path of rotation); and 2%. Results revealed positive effect of incorporating a positive level of blade camber to VAWT design. The most favorable configuration for the VAWT under study was determined to be the camber level that causes the camber line to coincide with the path of the rotor rotation. The paper presents an in-depth discussion of the flow physics and wake dynamics, for the two wind cases of VAWTs, through flow visualizations and blade force analysis.

Keywords: Blade camber, CFD, CP, Drag, Lift, NACA XX25, Steady wind, VAWT

Introduction

Due to the increasing awareness in energy security issues and climate change threats, most of the current research and development (R&D) programs in the energy sector are driven towards harnessing alternative energy sources. Wind energy, along with photovoltaic, solar

thermal, hydroelectric, biomass, and other resources, was given particular attention as a renewable and environmental-friendly energy resource. Its technological progress has been impressive over the years and because of its steady growth in competitiveness, it has developed into a mainstream energy source in many countries worldwide. Two main technologies are considered in the wind energy domain: the horizontal axis (VAWTs) and vertical axis wind turbines (VAWTs). For the past years, HAWTs have received significant R&D work and have become a mature technology making it a common choice for large scale wind power generation [1]. Conversely, VAWTs have not been given the same attention even though they present several advantages over HAWTs, especially for small scale power production [2] and when operating at low Reynolds numbers (Re). It is apparent in literature that accurate airfoil data to describe aerodynamics of VAWTs are very few. VAWT analyses are limited to a narrow number of blade profiles, substantially some NACA series symmetrical airfoils, for which low Reynolds numbers extended databases are available in technical literature [3]. The reason behind this is that most airfoil databases used for VAWT analysis are derived from aeronautical applications, where high angle of attack (α) are seldom encountered [4], and which hardly extend beyond stall, referring to relatively high Re ($>10^6$) [5]. With this, the current study aims to contribute to the efforts in filling in the gaps data in the literature of VAWT performance.

Aerodynamics of a Darrieus-based VAWT

Since the success of all wind energy conversion systems is largely dependent on maximizing their energy extraction, rotor aerodynamics plays a critical role in the minimization of the cost of energy they generate [3]. Figure 1 shows the velocities and forces driving a Darrieus VAWT.

Two important velocities are shown, namely: V_b or the velocity of the airfoil relative to the shaft that is always parallel to the chord c , having a magnitude equal to rotational speed ω multiplied by the radius R ; and U_∞ or the velocity of the wind, which is approximated at constant velocity in one direction. The resultant of these two velocities is W , which is the velocity of wind relative to the airfoil. The angle between W and V_b is the angle of attack α [2], [6].

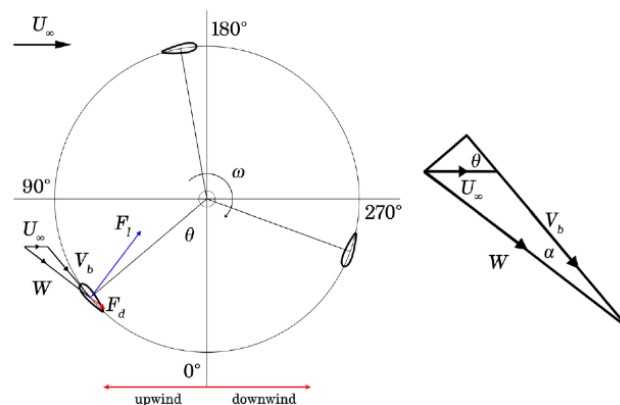


Figure 1. Forces on a darrieus-based VAWT [2]

W fluctuates from a maximum of $(\lambda+1)U_\infty$ to a minimum of $(\lambda-1)U_\infty$, where λ is the tip speed ratio equal to the ratio between V_b and U_∞ . At the same time, the angle of attack α also varies periodically between positive and negative values. From geometrical considerations, the W and α can be calculated using Equation 1 and Equation 2, respectively:

$$W = U_\infty \sqrt{1 + 2\lambda \cos\theta + \lambda^2} \quad (1)$$

$$\alpha = \tan^{-1} \frac{\sin\theta}{\lambda + \cos\theta} \quad (2)$$

where θ is the azimuth angle or the orbital blade position.

Aerodynamic lift F_l and drag F_d are generated when an incidence of wind flow on the turbine blades is present (i.e. $\alpha \neq 0$). In the 0° azimuth and the 180° position where $\alpha = 0^\circ$, F_l is zero and only F_d exists. F_l begins to be generated as the blades rotate out of these two positions and α changes. Both of these forces have components along the tangential (F_T) and normal (F_N) directions. The normal components of these forces do not influence the energy generation of the rotor but are a key factor when it comes to structural considerations [2]. The tangential components are the primary driving forces that dictate the performance of the VAWT and give rise to the instantaneous blade torque T_b (Equation 3).

$$T_b = (F_l \sin \alpha - F_d \cos \alpha)R \quad (3)$$

The instantaneous blade power P_b and rotor power P_B is computed as:

$$P_b = \omega T_b \quad (4)$$

$$P_B = \omega(T_{b,1} + T_{b,2} + T_{b,3}) \quad (5)$$

The instantaneous wind power on the other hand is given by Equation 6:

$$P_w = \frac{1}{2} \rho A U_\infty^3 \quad (6)$$

where A is the VAWT swept area, that is equal to the rotor diameter D multiplied by the blade length L , and ρ is the density of air. The instantaneous power coefficient CP can now be computed by dividing P_B by P_w .

$$CP = \frac{P_B}{P_w} \quad (7)$$

Under steady wind conditions, the VAWT CP is normally computed by averaging the instantaneous blade torque over one rotor rotation thus making the CP independent of azimuth position and giving a single-valued metric of the VAWT performance [2].

Blade Camber

The effect of airfoil asymmetry on the aerodynamics and performance of VAWT under steady wind condition was investigated in this paper. Airfoil asymmetry was achieved by applying various levels of camber (0.5%, 1.5% and 2%) to a four-digit NACA airfoil pro-file.

NACA XX25 airfoil profile, cambered at four different levels, was considered in the study. An illustration of the blade profiles evaluated is summarized in Figure 2.

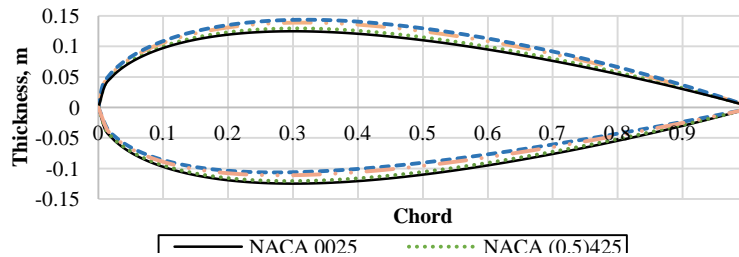


Figure 2. Symmetric and cambered NACA XX25 profiles

Each blade profile was tested with VAWT and optimum level of blade camber was determined through numerical simulation—a less expensive way of analyzing and improving the aerodynamics of wind turbines when compared to actual experimental tests [7]. Specifically, this was carried out using computational fluid dynamics (CFD) modeling.

Aerodynamic Performance of Various Airfoil Profiles

The availability of aerodynamic performance data for symmetric airfoils made them a common choice for VAWT applications. The performance of NACA airfoils has been investigated as early as 1937 by Jacobs & Sherma. Their study is a systematic investigation of representative groups of NACA airfoil profiles in a wide range of Reynolds numbers using static airfoil tests of lift and drag. In 1978, Healy [9], [10] conducted studies on the effects of airfoil thickness and camber on VAWT performance using multiple streamtube model. Results showed that thicker profiles are more preferable at lower Reynolds numbers and that higher output and smoother power curves are obtained with profiles closer to symmetric. The former however was contradicted by Danao et al. [11] in their CFD study on blade thickness and camber where thinner airfoils were found to produce higher values of lift through stronger pressure gradients. Moreover, cambered sections were found to improve the overall performance of thick airfoils. Slight camber along the blade path is seen to be desirable while inverted configurations are detrimental to power extraction especially in the downwind.

A comprehensive experimental dataset of symmetric NACA airfoils for VAWT applications was published by Sheldahl and Klimas [4]. The airfoil section data requirements for application to VAWTs are in fact broader in scope than those the aircraft industry [5]. The maximum value of angle of attack that a VAWT blade section is exposed to normally exceeds 25° especially near the ends of the curved blades of the traditional troposkein design of the Darrieus concept. Static airfoil tests were conducted and an extrapolation code was developed to generate performance data at Reynolds numbers outside the experimental range most especially at the low end where much of the operating conditions exist. Primarily the effect of blade thickness on symmetric NACA profiles was studied from 0° to 180° angle of attack and data for both increasing and decreasing incidence was taken to show hysteresis of airfoil performance.

Further, performance of cambered airfoils has been analyzed by Baker [12] and Kirke [13]. It was concluded that the use of cambered or angled blade profile can maximize power extraction. Such profiles can significantly increase the performance in the upwind where most of the power is produced. This also improves the VAWTs self-starting capabilities since cambering pushes the performance curve to lower λ . At low Reynolds number conditions, a separation bubble evolving at the leading edge is inevitable. Reattachment on the trailing edge needs to be encouraged to negotiate the pressure rise and sustain

the lift prior to full stall. A section with a more rounded nose and cambered leading edge is argued to accomplish the job.

McIntosh [14] carried out parametric studies in 2009 made using a free vortex model code. Results showed that thinner aerofoils produce higher maximum CP versus thicker sections. It was observed that NACA0012 CP curve had a sharp drop from the maximum point on both sides while thicker profiles display flatter top and gentler rounded drop in CP. Maximum CP was also observed to shift to lower λ . Thicker aerofoils are desirable in windy conditions because turbines operating at lower tip speed ratios will experience smaller fluctuations in λ during the gusts and the drop in CP is also reduced.

Computational Fluid Dynamics

Computational Fluid Dynamics (CFD) offers the best solution in VAWT performance simulation in comparison to momentum and vortex models [15]. The entirety of the flow is calculated by this model through numerically solving the Navier-Stokes equations. Navier-Stokes equations are a set of non-linear, coupled, partial differential equations for which an exact solution still does not exist. For the simulation of a wind turbine, the equations include the continuity equation and momentum equations. Turbulence is considered using the Reynolds-averaged Navier-Stokes equations where the introduction of a new term representing the turbulent stress gives rise to a number of turbulence models. Because of its flexibility, CFD has been gaining popularity for analyzing the complex, unsteady aerodynamics involved in the study of wind turbines and has demonstrated an ability to generate results that compare favorably with experimental data. CFD has shown no problems predicting the performance of either high or low solidity wind turbines or for various tip speed ratios. However, it is important to note that predicting the performance of a wind turbine using CFD typically requires large computational domains with sliding interfaces and additional turbulence modelling to capture unsteady effects, therefore, CFD can be computationally expensive [16].

Methodology

Mesh Generation

The physical model of the VAWT and the surrounding domain was represented in a two-dimensional grid. An illustration of the 2D CFD model used in the study is shown in Figure 3. The effects of the blade-support arm and blade ends were neglected.

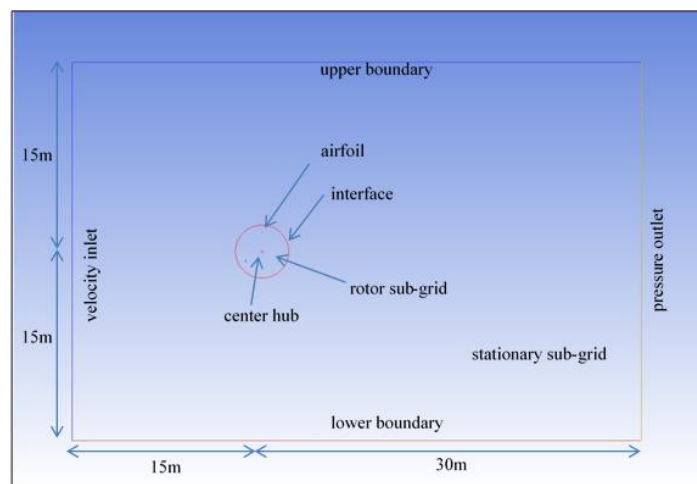


Figure 3. Two-dimensional CFD model

Moving sub-grids were considered in this study since it primarily deals with a rotating machine. The 2D computational domain was divided into two distinct sub-grids, namely: 1) stationary sub-grid that is the rectangular outer zone, determining the overall calculation domain, with a circular opening centered on the turbine's rotational axis; and 2) rotor sub-grid that is a circular inner zone, which shall rotate with rotor angular velocity. The location of the rotor sub-grid coincides exactly with the circular opening inside the stationary sub-grid area and centered on the turbine rotational axis.

The work is aimed at simulating the operation of the VAWT in an open field condition, hence boundaries were positioned far enough from the rotor test section to avoid solid blockage and to allow full development of the wake. In this study, the side wall and inlet distances were set to 5 diameters away from the rotor while outlet distance was set to 10 diameters away as suggested for testing VAWT in open field scale [2], [17]. The geometry and mesh of the model was generated by importing the airfoil coordinates of the NACA XX25 into the ICEM CFD 14.5 software.

One of the critical factors that dictate the overall quality of the computational domain is the spatial resolution of the mesh near the blade. To obtain reliable results of forces on the blade surfaces, appropriate number of airfoil nodes and cell growth rate are needed to be considered. To determine the appropriate surface node density, initial runs were done wherein three surface node densities were tested at $\lambda = 4$, and the blade torque coefficients in one full rotation for each case were compared.

Figure 4 shows the result of the node density study for one complete rotation. As can be seen in the graph, while the torque curve of the mesh with 70 airfoil nodes greatly deviates from the other two curves, there is a very close agreement observed between the curves of the meshes with 210 and 300 airfoil nodes, such that they are already overlapping in most areas. The ΔCP computed between the two cases was only 0.0025 or 0.825% difference in magnitude. Given this very minimal variation between the two, 210 airfoil nodes was chosen since it can give accurate results at a lesser computational time.

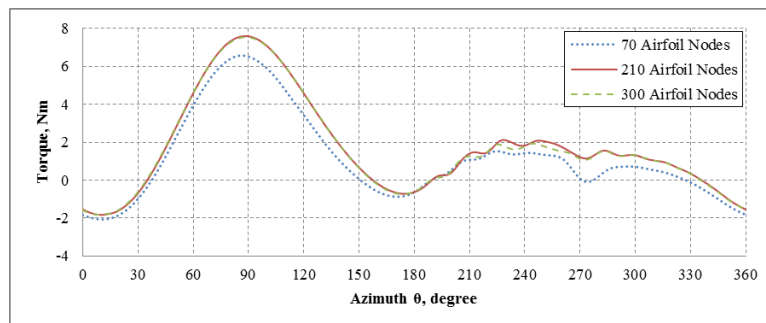


Figure 4. Node density study at $\lambda = 4$

Each blade of the rotor has a chord length of 0.15m and was meshed with 210 nodes, with clustering both in the leading and trailing edges where high gradients in pressure and flow were expected. In creating the rotor sub-grid (Figure 5), an O-type block was first created around the airfoil from which the cells were generated. The first cell height was set ensuring a y^+ not exceeding 1. The cells expand from the wall to the O-type block boundaries with a growth rate of 1.1, giving a minimum of 90 layers within the said block. Cells beyond this block were set to have a maximum cell height not to exceed 0.10c for the rotor sub-grid. A smoothing algorithm in the meshing software was used to reduce the angle skewness of the cells.

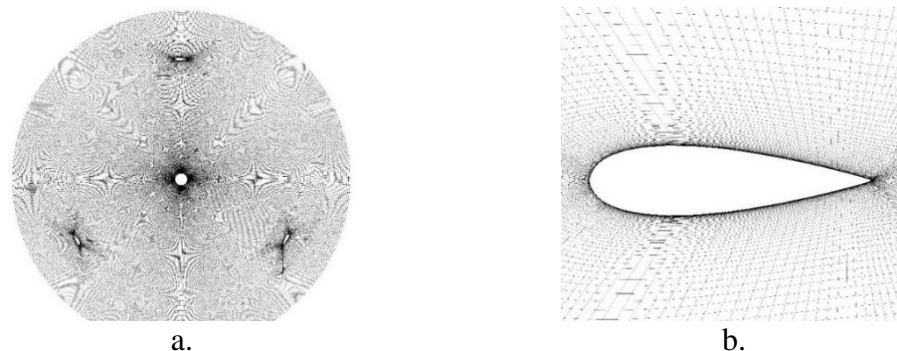


Figure 5. Details of rotating mesh: (a) rotor sub-grid and (b) near-blade mesh

The outer stationary sub-grid (Figure 6) on the other hand, was meshed relatively coarser than the rotor sub-grid. Minimum cell height was set to one chord length. Cell growth height from the circular interface to the wall boundaries was to 1.1 giving a maximum cell height of 0.25m. Coarser meshes reduce computational time.

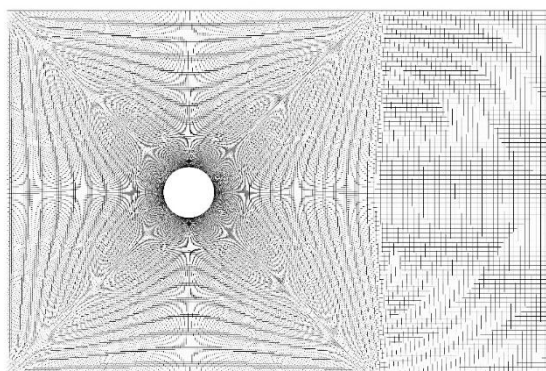


Figure 6. Stationary sub-grid

CFD Solver

The CFD software FLUENT v14.5, which uses the finite volume method was employed in this study to simulate the fluid flow through the VAWT. It is understood from the BEM theory that the whole blade can be thought to be made up of finite blade elements. Hence, a 2D CFD model which can be considered to be an elemental section of the blade shall be used in the simulation. Moreover, based from previous studies, 2D model has been found to be sufficient in demonstrating various factors that influence the performance and majority of flow physics of VAWT.

The computational domains generated were read into the CFD code FLUENT for numerical iterative solution. All simulations to be done shall be carried out using this CFD program. The rotational motion was simulated by allowing the rotor sub-grid to rotate at constant angular velocity. The mesh movement was defined explicitly by specifying time-varying positions for all the rotor sub-grid block cell vertices. An interface boundary surrounding the rotating sub-grid within the model was allowed to slide at specified velocity to represent its relative motion to the stationary sub-grid.

The coupled pressure-based solver was selected with a second order implicit transient formulation for improved accuracy. All solution variables were solved using second order

upwind discretization scheme since most of the flow can be assumed to be not in line with the mesh.

VAWT performance simulations were done under steady wind conditions, at a constant free stream of $U_\infty = 5\text{m/s}$, over a range of tip speed ratios from 1 to 5 in increments of 0.5, both for the symmetrically and asymmetrically bladed VAWTs. The VAWT was allowed to run for 10 rotations in each simulation and T_b of one blade was monitored all throughout. The maximum iteration per time step was set to 50 to make each physical time step converge. Time step convergence was monitored for all conserved variables and it was observed that acceptable levels of residuals (less than 1×10^{-4}) were attained after 8 rotor rotations, also achieving periodic convergence. For illustration, the T_b curve of the symmetric bladed VAWT at $\lambda = 4$ for 10 rotations is plotted in Figure 7. The peaks of the upwind torque for cycles 9 and 10 are level and the downwind ripple match closely. The difference in average torque between cycle 9 and cycle 10 for all λ cases averages to about 1.5% with highest percentage difference at the maximum $\lambda = 5$ (~8%) and lowest at the minimum $\lambda = 1$ (~0.1%).

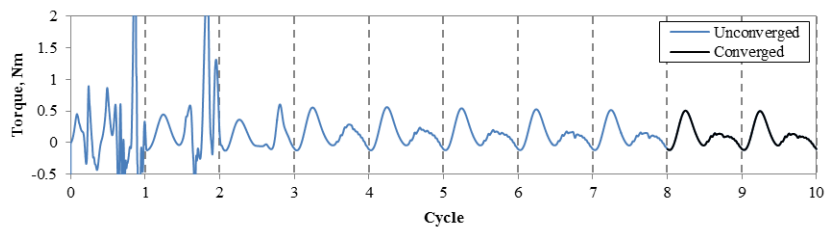


Figure 7. T_b ripple over 10 full rotor rotations at $\lambda = 4$

Model validation was carried out by comparing the current CFD model to the QR5 wind tunnel test results as cited by Scheurich [16] and to the results of the DMS model by Wahl [18]. As seen in Figure 8, the current model compares well with the two other models in terms of the general trend of CP curve with optimum CP occurring at $\lambda = 3.5-4$. Close results are observed between the current and Wahl's models, with minimal variation which can be attributed to the difference in numerical model used – DMS vs. CFD. On the other hand, though very similar trend was also observed from the results of the wind tunnel experiment of QR5, its relatively high CP magnitudes may be due to its optimized blade configuration, which is helically twisted.

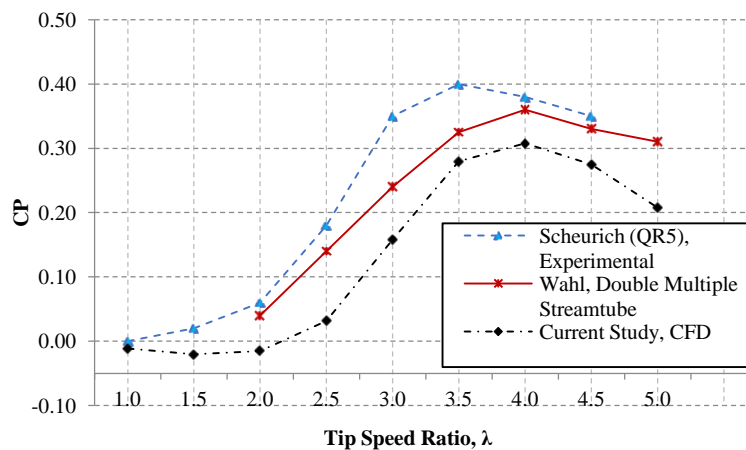


Figure 8. CP curves vs. λ of various NACA 0025-bladed VAWTs

Results and Discussion

Power Coefficient

Four variations of blade camber level of VAWT were tested in this study, namely: 0% (symmetric); 0.5%; 1.5% (camber along the blade path); and 2%. The results of the simulations for all these VAWT profiles is summarized in Figure 9, showing the corresponding power coefficient (CP) curve of each case. Generally, a region of negative trough is present in all CP curves, specifically in regions within $1 > \lambda > 2$, giving negative CP values within this low range of λ . After this portion, the CP tends to increase until it reaches a peak at $\lambda = 4$ that is also common for all the blade profiles evaluated. CP gradually decreases afterwards.

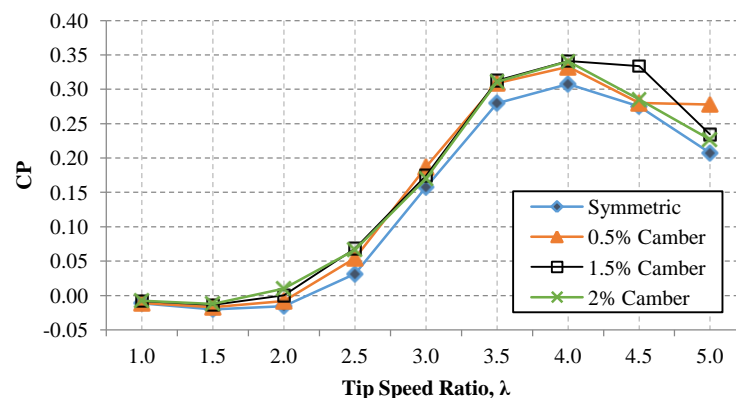


Figure 9. CP curves

Results show that incorporating a positive level of camber to the design of VAWT blades can improve its overall performance. All camber-bladed VAWTS gave higher values of CP as compared to the symmetrically-bladed VAWT. The blade with 1.5% level of camber performed best, gaining the highest CP for almost all the range of λ evaluated. Maximum CP is predicted at 0.3410 for the said blade profile which is relatively higher than the predicted maximum CP of the other blade profiles ($CP = 0.3409$ for 2% camber, $CP = 0.333$ for 0.5% camber and $CP = 0.308$ for the symmetric blade). A 10% difference in efficiency is observed between the best and the least blade profiles. In the succeeding discussion, the best performing blade profile (blade with 1.5% camber level) is analyzed further, comparing its performance to the symmetric blade that was chosen as baseline model.

Torque, Lift and Drag Coefficients

The variation of torque versus the azimuthal position of blade at steady wind $U_\infty = 5$ m/s for one full rotor rotation are shown in Figure 10 and Figure 11. The following discussion is true for both the symmetric and 1.5% camber-bladed VAWT. As observed from the graphs, blade torque tends to increase from $\lambda = 1$ to $\lambda = 4$ and drops afterwards, giving lower values of blade torque at $\lambda = 4.5$ and $\lambda = 5$. Stalling in the upwind was also observed to be gradually delayed as λ increases. Downwind performance is seen to improve as λ increases resulting in the steady increase in CP (from $\lambda = 1$ to $\lambda = 4$). Torque in the downwind can be observed to be highest at $\lambda = 3.5$ followed only by torque magnitudes at $\lambda = 4$. However, torque in the upwind is higher at higher λ (i.e. $\lambda = 4, 4.5$ and 5) than the other λ as compared to that of $\lambda = 3.5$, which results in a higher CP at $\lambda = 4$. Upwind performance

is very similar for $\lambda = 4$, $\lambda = 4.5$ and $\lambda = 5$. The main factor for the lower CP at $\lambda = 4.5$ and $\lambda = 5$ is the poorer performance in the downwind side.

By analyzing the torque and the aerodynamic lift and drag forces acting on the blades, the behaviour and performance of VAWT at various λ can be better understood and explained [2]. In the purpose of clearly presenting the significant differences among the range of λ tested in terms of overall performance, two extreme conditions were considered for analysis. At $\lambda = 2$ and $\lambda = 4$, the curves of T_b against θ and the curves of C_l and C_d against α were plotted and compared.

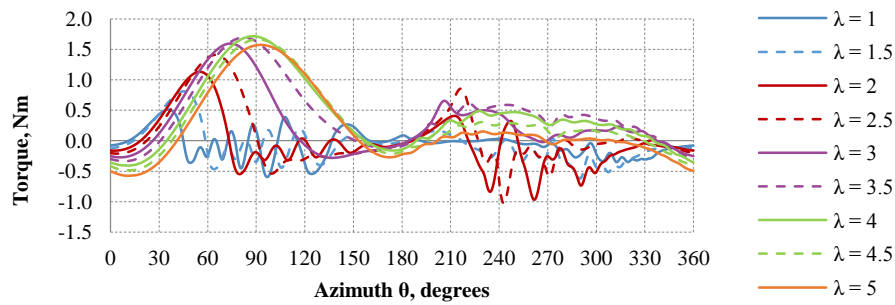


Figure 10. T_b ripple of the symmetric-bladed VAWT at $U_\infty = 5$ m/s

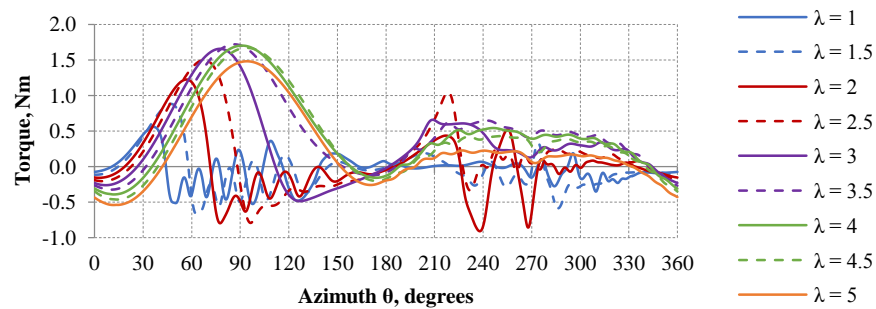


Figure 11. T_b ripple of the 1.5% camber-bladed VAWT at $U_\infty = 5$ m/s

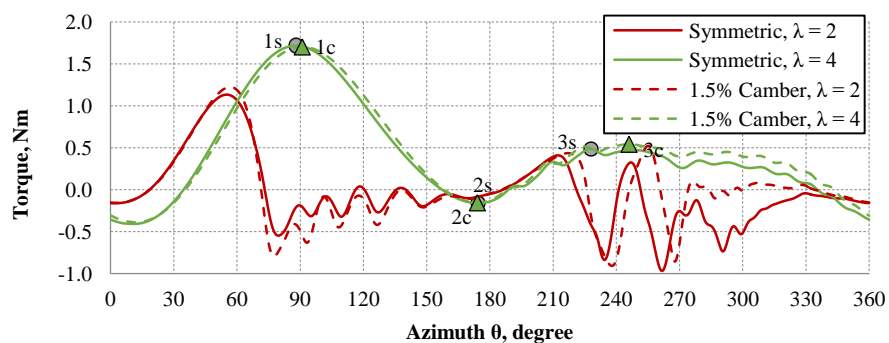


Figure 12. T_b ripple of VAWT for two λ cases at $U_\infty = 5$ m/s

Figure 12 shows the blade torque curves of VAWT for the two λ cases at $U_\infty = 5$ m/s. It can be seen from the figure that the performance of both the symmetric and camber-bladed VAWTs at $\lambda = 4$ is significantly better than at $\lambda = 2$ giving a maximum T_b that is approximately 50% higher than the maximum T_b of the latter. Maximum T_b recorded at $\lambda = 2$ and $\lambda = 4$ for the symmetrically bladed VAWT were 1.13 Nm and 1.72 Nm, respectively. For the 1.5% camber-bladed VAWT, higher maximum T_b was recorded for $\lambda = 2$ at 1.23 Nm

and a slightly lower T_b for $\lambda = 4$ at 1.70 Nm. Stalling, as mentioned earlier, is much delayed for higher λ while shedding of vortices is indicated by the ripple of T_b at the lower λ . The very low calculated CP at $\lambda = 2$ can be attributed to the range of T_b for this lower λ , which are mostly negative in value. These negative values of T_b are observable in regions $70^\circ < \theta < 180^\circ$ and $220^\circ < \theta < 360^\circ$. In contrast, the opposite is observed at $\lambda = 4$ with predominantly positive T_b . Moreover, it is noticeable in the graph that at $\lambda = 2$, the symmetrically bladed VAWT performs better than the camber-bladed VAWT in the upwind side, especially within the azimuthal range $70^\circ < \theta < 165^\circ$. However, higher values of T_b were recorded on the downwind side ($250^\circ < \theta < 365^\circ$) of the camber-bladed VAWT that offset the effect of the lower T_b values on the upwind side, thus giving higher CP for the said VAWT profile. At $\lambda = 4$, the performance of the camber-bladed VAWT is obviously much better than the other VAWT profile giving higher values of T_b that commenced from $\theta = 90^\circ$ to $\theta = 360^\circ$.

The maximum T_b for the rotation is represented in Figure 12 by point 1s for the symmetrically bladed VAWT and point 1c for the 1.5% camber-bladed VAWT. Point 1s is located on the upwind side at $\theta = 88^\circ$ with $\alpha = 13.9^\circ$ and $T_b = 1.72$ Nm. The lift at this location is $C_l = 0.85$ (Figure 13). This value is among the highest values of lift generated for the rotation. For the 1.5% camber-bladed VAWT on the other hand (Figure 14), the maximum torque was predicted to be $T_b = 1.70$ Nm at $\theta = 91^\circ$ and $\alpha = 13.9^\circ$. At this location, lift $C_l = 0.81$. As discussed from the previous section, the maximum torque for the camber-bladed VAWT is slightly lower than the symmetric VAWT but better performance of the former on the downwind side resulted to its higher values of CP . Lift coefficients at points 1s and 1c are both lower in magnitude compared to the XFOIL derived static data for the two NACA XX25 airfoils. The NACA 0025 predicted static stall lift coefficient is $C_{l,ss} = 1.13$ at an angle of attack $\alpha = 10.75^\circ$. This value is 25% higher in magnitude than the corresponding lift coefficient of the NACA 0025 airfoil in the dynamic case. This is also true with the 1.5% cambered blade (NACA 1425) with higher static stall lift of $C_{l,ss} = 1.14$ at $\alpha = 9^\circ$, an 80% difference in magnitude compared to the same blade profile subjected under pitching motion (Figure 14). According to Lee et al. [16] as cited by Danao [2], the lift force on an airfoil under pitching motion is increased as an effect of dynamic stalling. However, the opposite was observed from the plotted data, showing higher static stall lift coefficients, which can be attributed to the overestimation of the software XFOIL that was used to predict the static data of the airfoils. Moreover, these static data were acquired at $Re = 200,000$ that is slightly higher than the actual Reynold's number for the same blade profile at $\lambda = 4$ which is $Re = 160,000$. What is still evident from the lift curves is that even after static stall angle, lift in the dynamic curves continues to increase as an effect of vortex separation from the airfoils due to dynamic stalling [17]. This effect is more obvious under low values of λ as can be seen from Figure 13 and Figure 14 where the curve of $\lambda = 2$ has higher maximum lift than that of $\lambda = 4$ at even higher value of α for both blade profiles. Despite the high lift, T_b is negative at this point in the case of $\lambda = 2$ for both blade profiles because of the overpowering effect of drag (see Figure 15 and Figure 16). The predicted static stall drag coefficients for the symmetric and cambered airfoil are $C_{d,ss} = 0.03$ and $C_{d,ss} = 0.02$, respectively. These are comparatively lower than the drag coefficient of the symmetric (Point 1s in Figure 15) and cambered (Point 1c in Figure 16) airfoils under dynamic condition, which is $C_d = 0.10$ for both blade profiles.

The values of T_b at $\lambda = 4$ then gradually decrease down to the negative region after point 1 with minimum at Point 2s ($\theta = 174.5^\circ$, $\alpha = 1.83^\circ$) for symmetric blade and point 2c ($\theta = 174^\circ$, $\alpha = 1.99^\circ$) for cambered blade. At this point, the XFOIL predicted static C_l for the symmetric blade is roughly 0.18. Though this static lift is relatively high, dynamic lift drastically dropped from point 1 to a negligible value of -0.04 at point 2, an outstanding

decrease in magnitude of about 0.89. The corresponding drag, on the other hand, was minimally lowered by only 0.08. T_b at this point is -0.161 Nm as reflected by this comparatively high drag and insignificant lift. Similarly, for the blade with camber, T_b is negative but is slightly higher than the former at -0.157 Nm. Lift is also negligible at $C_l = -0.06$ with a corresponding drag of $C_d = 0.02$.

Points 3s ($\theta = 228^\circ$, $\alpha = -12.58^\circ$) and 3c ($\theta = 246^\circ$, $\alpha = -14.26^\circ$), on the other hand, represent the maximum values of T_b on the downwind side for the symmetric and cambered blades, which are 0.49 Nm and 0.54 Nm, respectively. These are both located in the third quadrant just before $\theta = 270^\circ$, the location where the blades interact with the center hub wake. The α for both blade profiles at this point should bring them into dynamic stall but lift and drag are lower at $C_l = -0.587$ and $C_d = 0.053$ for symmetric blade and $C_l = -0.590$ and $C_d = 0.072$ for cambered blade. Lift and drag are generally lower in this region since most of the power from the wind was already extracted on the upwind side of the rotation.

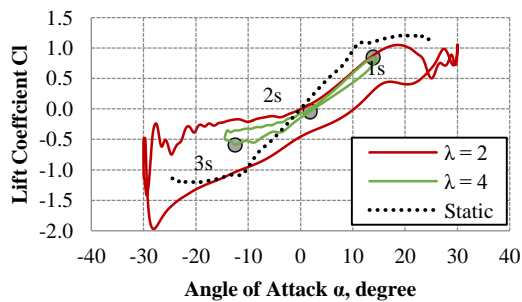


Figure 13. Lift coefficient of symmetric-bladed VAWT for two λ cases at $U_\infty = 5\text{m/s}$

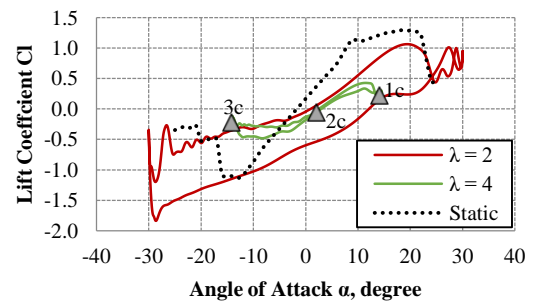


Figure 14. Lift coefficient of camber-bladed VAWT for two λ cases at $U_\infty = 5\text{m/s}$

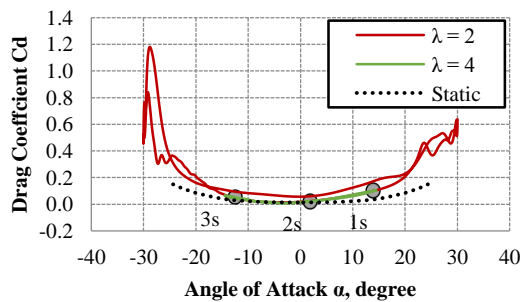


Figure 15. Drag coefficient of symmetric-bladed VAWT for two λ cases at $U_\infty = 5\text{m/s}$

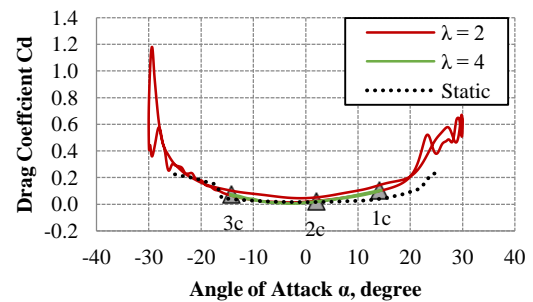


Figure 16. Drag coefficient of camber-bladed VAWT for two λ cases at $U_\infty = 5\text{m/s}$

Flow Visualizations

Under steady wind conditions, monitoring of flow was done over one blade only. Similar results are expected of all three blades of the rotor due to its symmetry hence, monitoring one blade will be sufficient enough to visualize the effect of wake and vorticity on its performance. Z-vorticity was calculated for cases of camber level (0% and 1.5%) and vorticity contours are presented at $\lambda = 2$.

Figure 17 shows the z-vorticity profiles of one blade for each of the two VAWT configurations on the upwind side of rotation. At $\lambda = 2$, no visible separation of flow on the blade surface is observed in the azimuthal position $\theta = 30^\circ$ for both blade profiles as torque

T_b continuous to gain in magnitude that has started from $\theta = 20^\circ$ (Figure 12), peaking just before $\theta = 60^\circ$. Flow separation partially develops on the pressure side of the blades as they cross $\theta = 60^\circ$ where T_b values started to drop, causing stalled flow. At $\theta = 90^\circ$, the flow is fully separated from the blade surface and vortices are shed both at the leading and trailing edges. This separation can be associated with the rapid drop in the magnitude of T_b from $\theta = 60^\circ$ to $\theta = 80^\circ$ (Figure 12). Detached flow continued to $\theta = 120^\circ$ resulting in the observed vortex shedding until mid-rotation at $\theta = 180^\circ$ that can be related to the negative torque within this range. The flow is seen to briefly reattach in the downwind side (see Figure 18) of rotation at $\theta = 210^\circ$ where torque is high in value, but continued to shed vortices afterwards until $\theta = 330^\circ$ where the flow reattached to blade once more which is reflected by the significant negative T_b fluctuations within this region. The relatively large angles of attack under $\lambda = 2$ caused the poor performance of the VAWTs since it generates large scale of vortex shedding. Moreover, z-vorticity images are very similar for both blade profiles for almost all the θ . Only a minor difference can be observed such that fluid flow is slightly more attached to the camber blade that are more obvious in the regions with vortex shedding, especially between $120^\circ < \theta < 300^\circ$. This can be the reason for a better performance of the VAWT with camber blades.

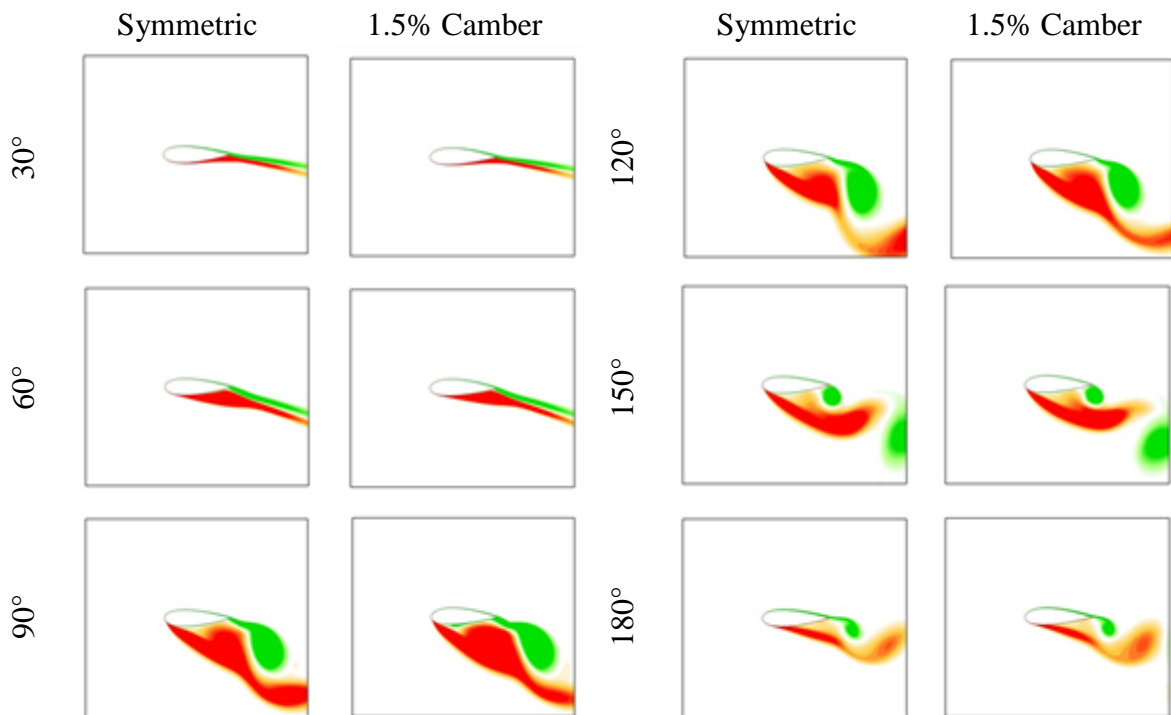


Figure 17. Z-vorticity profiles in the upwind side for the two cases

Z-vorticity images generated for the same VAWT profiles subjected under $\lambda = 4$ are not shown for brevity. However, it is observed that the flow are more attached to the blades all throughout the rotation. This can be associated with mostly positive values of T_b for this λ (between $40^\circ < \theta < 150^\circ$ and $200^\circ < \theta < 330^\circ$) that are remarkably high at $\theta = 60^\circ$ to $\theta = 120^\circ$ (Figure 12). The high values of T_b on the upwind side of rotation are due to the unperturbed wind and near static stall α that the blade sees. T_b became considerably low only after $\theta = 150^\circ$ up to $\theta = 190^\circ$ where T_b values are negative. This can be explained by the wake that is seen by the blade in this azimuthal position, which was generated by the other foregoing blade. On the other hand, the relatively low flat positive values of T_b in the downwind region, specifically between $200^\circ < \theta < 330^\circ$ are due to the reduced wind flow

velocity as a result of wind power extraction on the upwind side. No observable difference can be perceived between the set of generated z-vorticity profiles of the camber and symmetric blades.

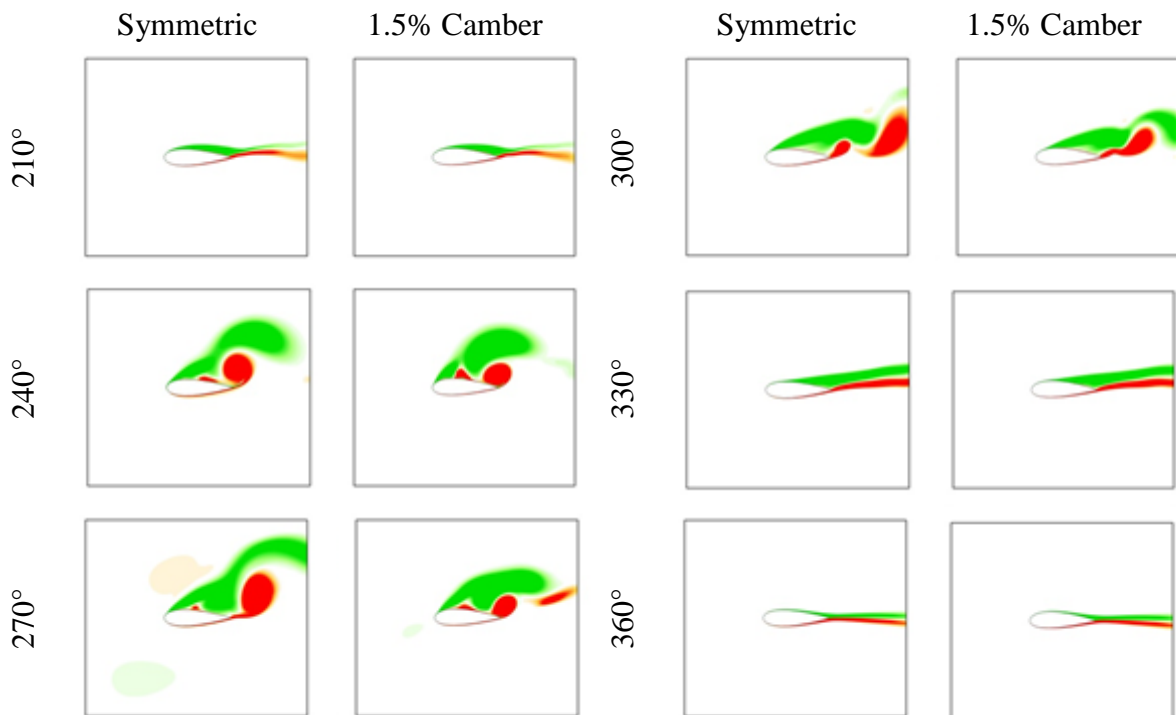


Figure 18. Z-vorticity profiles in the downwind side for the two cases

Conclusions

The study was aimed at evaluating the effects of introducing camber to the design of blades of a VAWT. This was carried out by comparing the performance of VAWT with NACA XX25 blades, cambered at 0.5%, 1.5% (cambered following path curvature) and 2%, to the performance of their symmetric-bladed VAWT counterpart. The RANS-based CFD modeling was used in the process, through the commercial software ANSYS FLUENT v14.5. Investigation was carried out by simulating VAWT performance under steady wind. Simulations were done over a range of λ (1 through 5, at increments of 0.5) at a constant $U_\infty = 5\text{m/s}$. Results showed that for all the evaluated configurations of VAWT, the maximum CP occur when $\lambda = 4$. Moreover, all camber-bladed VAWTs have been found to perform better than the symmetric-bladed VAWT, having higher CP for all the range of λ evaluated. The blade with 1.5% level of camber, on the other hand, performed best with the highest predicted CP for almost all the range of λ . For said blade profiles, the maximum CP was predicted to be higher at 0.3410, versus the predicted maximum CP for the other three VAWT profiles ($CP = 0.3409$ for 2% camber, $CP = 0.333$ for 0.5% camber and $CP = 0.308$ for the symmetric). A 10% difference in efficiency was recorded between the best and the worst blade profiles.

Acknowledgement

This research study was funded and supported by the ERDT Scholarship Program of the Department of Science and Technology through the University of the Philippines – College of Engineering.

References

- [1] Global Wind Energy Council, "Global Statistics," [Online]. Available: <http://www.gwec.net/global-figures/graphs/> [Accessed: May, 2014]
- [2] L.A.M. Danao, *The Influence of Unsteady Wind on the Performance and Aerodynamics of Vertical Axis Wind Turbines*, Thesis(PhD), The University of Sheffield, United Kingdom, 2012.
- [3] M.R. Castelli, S. De Betta, and E. Benini, "Effect of blade number on a straight-bladed vertical-axis darreius wind turbine," *International Journal of Aerospace and Mechanical Engineering*, Vol. 6, pp. 256–262, 2012.
- [4] R.E. Shedahl, and P.C. Klimas, *Aerodynamic Characteristics of Seven Symmetrical Airfoil Sections through 180-Degree Angle of Attack for Use in Aerodynamic Analysis of Vertical Axis Wind Turbines*, SAND80-2114, Sandia National Laboratories, Albuquerque, New Mexico, 1981.
- [5] M.R. Castelli, G. Simioni, and E. Benini, "Numerical analysis of the influence of airfoil asymmetry on vawt performance," *International Journal of Aerospace and Mechanical Engineering*, Vol. 6, pp. 76–85, 2012.
- [6] H. Beri, and Y. Yao, "Double multiple stream tube model and numerical analysis of vertical axis wind turbine," *Energy and Power Engineering*, Vol. 2011, No. 3, pp. 262–270, 2011.
- [7] A.M. Biadgo, A. Simonovic, D. Komarov, and S. Stupar, "Numerical and analytical investigation of vertical axis wind turbine," *FME Transactions*, Vol. 41, No. 1, pp. 49–58, 2013.
- [8] E. Jacobs, and A. Sherma, *Airfoil Section Characteristics as Affected by Variations of the Reynolds Number*, NACA, Washington, D. C., 1937.
- [9] J.V. Healy, "The influence of blade camber on the output of vertical axis wind turbines," *Wind Engineering*, Vol. 2, No. 3, pp. 146–155, 1978.
- [10] J.V. Healy, "The influence of blade thickness on the output of vertical axis wind turbines," *Wind Engineering*, Vol. 2, No. 1, pp. 1–9, 1978.
- [11] L.A.M. Danao, N. Qin, and R. Howell, "A numerical study of blade thickness and camber effects on vertical axis wind turbines," In: *Proceedings of the Institution of Mechanical Engineers, Part A: Journal of Power and Energy*, Vol. 226, No. 7, 2012.
- [12] J.R. Baker, "Features to aid or enable self-starting of fixed pitch low solidity vertical axis wind turbines," *Journal of Wind Engineering and Industrial Aerodynamics*, Vol. 15, pp. 369–380, 1983.
- [13] B.K. Kirke, *Evaluation of Self-Starting Vertical Axis Wind Turbines for Stand-Alone Applications*, Thesis(PhD), Griffith University, Gold Coast, Australia, 1998.
- [14] S.C. McIntosh, H. Babinsky, and T. Bert, "Aerodynamic Modeling of Swept Bladed Vertical Axis Wind Turbines," American Institute of Aeronautics and Astronautics, Inc., Orlando, Florida, 2009.
- [15] M.C. Claessens, *The Design and Testing of Airfoils for Application in Small Vertical Axis Wind Turbine*, Thesis (Master's), Delft University of Technology, 2006.
- [16] T.J. Carrigan, *Aerodynamic Shape Optimization of a Vertical Axis Wind Turbine*, Thesis (Master's), The University of Texas at Arlington, 2010.
- [17] M.R. Castelli, A. Englaro, and E. Benini, "The Darrieus wind turbine: proposal for a new performance prediction model based on CFD," *Energy*, Vol. 36, No. 8, pp. 4919–4934, 2011.
- [18] P. Gerontakos, and T. Lee, "Particle image velocimetry investigation of flow over unsteady airfoil with trailing-edge strip," *Experimental Fluids*, Vol. 44, pp. 539–556, 2008.
- [19] J.W. Larsen, S.R.K. Nielsen, and S. Krenk, "Dynamic stall model for wind turbine airfoils," *Journal of Fluids and Structures*, Vol. 23, pp. 959–982, 2007.